DOI: 10.26599/FSHW.2025.9250871

Contents lists available at SciOpen

Food Science and Human Wellness

journal homepage: https://www.sciopen.com/journal/2097-0765

China Food Publishing Co.

Colostrum Whey Protein Attenuates Osteoporosis via Osteogenic Stimulation, Anti-Resorptive Effects, and Hepatic-Bone Axis Modulation

Guozhi Ji[a], Shuzhen Cheng[b], Xinnuo Wang[a], Mati Ullah Khan[c], Lijun You[a, *]

[a] *School of Food Science and Engineering, South China University of Technology, Guangzhou, Guangdong, 510640, China*

[b] *National Engineering Research Center of Seafood, Collaborative Innovation Center of Seafood Deep Processing, Dalian Polytechnic University, Dalian 116034, China*

[C] *School of Agriculture Engineering and Food Science, Shangdong University of Technology, Zibo, 255049, China*

ABSTRACT: Osteoporosis, a prevalent skeletal disorder aggravated by estrogen deficiency, is a major global health concern that presents significant clinical challenges, particularly for postmenopausal women. This study evaluates the therapeutic potential of colostrum whey protein (CWP) in mitigating estrogen deficiency-induced osteoporosis through both *in vivo* (ovariectomized murine model) and *in vitro* (osteoblast culture) approaches. In ovariectomized (OVX) mice, CWP administration increased bone mineral density (BMD) by 45%, elevated trabecular number (Tb.N) by 38%, restored trabecular thickness (Tb.Th), and reduced trabecular separation (Tb.Sp) by 40%. Histomorphometric analysis confirmed enhanced trabecular structure, collagen restoration, and reduced osteoclast activity. CWP also restored bone metabolism by increasing alkaline phosphatase (ALP) and osteoprotegerin (OPG) levels, while decreasing receptor activator of nuclear factor kappa-B ligand (RANKL) and tartrate-resistant acid phosphatase (TRAP) levels. Mechanistic studies showed that CWP modulated the hepatic-bone axis through suppression of PP2ACα and induction of lecithin-cholesterol acyltransferase (LCAT), facilitating cholesterol transport. Furthermore, CWP upregulated osteogenic markers (bone morphogenetic protein-2 (BMP-2), runt-related transcription factor-2 (RUNX-2), and activated MAPK, BMP/Smad, and WNT/β-catenin signaling pathways, promoting osteoblast proliferation, differentiation, and mineralization *in vitro*. These findings highlight CWP's dual role in enhancing bone formation and inhibiting resorption through both local (osteoblast activation) and systemic (hepatic-bone axis modulation) mechanisms. Collectively, CWP emerges as a promising multi-target therapeutic candidate for osteoporosis, bridging bone remodeling and metabolic crosstalk. Additional translational studies are warranted to validate its clinical efficacy.

Keywords: colostrum whey protein; osteoporosis; bone metabolism; hepatic-bone axis; osteoblast;

1. Introduction

Osteoporosis, a metabolic bone disease characterized by diminished bone density and deterioration of bone microstructure, elevates fracture risk and continues to pose a major global health challenge, especially among postmenopausal females and the elderly [1-3]. The disease originates from an imbalance in bone remodeling, a dynamic process governed by osteoblast-mediated bone formation and resorptive osteoclasts,

***Corresponding author**
feyoulijun@scut.edu.cn

Received 12 June 2025
Received in revised from 28 July 2025
Accepted 29 August 2025

disrupted by hormonal changes (e.g., estrogen decline) and age-related cellular senescence [4,5]. At the molecular level, bone remodeling is coordinated by an interplay of signaling pathways: the canonical WNT/β-catenin pathway facilitates β-catenin stabilization and nuclear translocation to activate osteogenic transcription factors, while the BMP/Smad cascade regulates osteoblast differentiation through both Smad1/5/8-dependent phosphorylation and non-canonical MAPK signaling pathways [6-9]. Concurrently, osteoclastogenesis is controlled by the OPG/RANKL/RANK axis, which modulates precursor differentiation via NF-κB and AP-1 activation, and PI3K/Akt signaling, which enhances osteoclast survival and resorptive function [8-10]. Central transcriptional regulators include RUNX-2 and SP7 (Osterix), which drive osteoblast lineage commitment and matrix synthesis, and NFATc1, a calcium-sensitive transcription factor essential for osteoclast maturation [10].

The hepatic-bone axis has recently been recognized as a critical bidirectional regulator of skeletal and metabolic health. Hepatocyte-derived factors, including insulin-like growth factor-1 (IGF-1) and taurine, directly stimulate osteoblast proliferation and inhibit osteoclast activity, while bone-derived osteocalcin and fibroblast growth factor 23 (FGF23) reciprocally modulate hepatic glucose metabolism and cholesterol homeostasis [11]. Estrogen deficiency disrupts this crosstalk, triggering hepatic stellate cell activation, collagen deposition, and dysregulated lipid metabolism, all of which exacerbate bone loss and microarchitectural deterioration [12]. Estrogen's dual role in enhancing osteoblast survival via ERα-mediated PI3K/Akt activation and suppressing osteoclastogenesis through RANKL inhibition further underscores its systemic influence [10,12].

Colostrum whey protein (CWP), a bioactive component of bovine colostrum containing growth factors (IGF-1, TGF-β), immunoglobulins, and low-molecular-weight peptides, demonstrates osteoprotective efficacy in preclinical models [13]. Unlike conventional dietary interventions, such as fish collagen hydrolysates (primarily enhancing collagen synthesis) or milk-derived casein phosphopeptides (improving calcium absorption) [14-16], CWP uniquely integrates anabolic and anti-resorptive actions. It enhances trabecular bone volume and connectivity density, upregulates osteogenic markers (e.g., BMP-2, RUNX-2), and modulates systemic pathways involving hepatic cholesterol efflux and lipoprotein metabolism [13]. Current anti-osteoporotic therapies, including bisphosphonates and denosumab, predominantly target osteoclast inhibition but fail to address the anabolic deficits inherent in age-related and estrogen-deficient osteoporosis [17,18]. In contrast, CWP exhibits dual efficacy, stimulating osteoblast proliferation and differentiation via WNT/β-catenin and BMP/Smad activation while suppressing osteoclastogenesis through RANKL/OPG axis modulation, positioning it as a multitargeted therapeutic candidate [11,19].

This study investigates CWP's capacity to mitigate estrogen deficiency-induced osteoporosis in ovariectomized (OVX) murine models, with a focus on bone mineral density (BMD), trabecular microarchitecture (including Tb.Th and Tb.Sp), and hepatic-bone axis regulation. Mechanistically, CWP activates WNT/β-catenin signaling via LRP5/6 receptor phosphorylation, stabilizing β-catenin to promote osteoblast mineralization, and enhances BMP/Smad signaling through Smad1/5/8 complex formation.

Concurrently, it suppresses hepatic PP2ACα, a negative regulator of LCAT, thereby enhancing cholesterol transport and reverse cholesterol transport (RCT) to bone marrow stromal cells. These findings elucidate CWP's dual role as both an osteogenic enhancer and systemic metabolic modulator, bridging skeletal anabolism and hepatic lipid metabolism. This preclinical evidence positions CWP as a novel therapeutic strategy for osteoporosis, addressing both local bone remodeling deficits and systemic metabolic dysregulation.

2. Materials and Methods

2.1 Materials

CWP is a powder (≥ 80% protein content) prepared by collecting colostrum from cows within 3 days after calving, followed by removal of fat, casein, and lactose through processing including defatting, isoelectric point precipitation, microfiltration, and drying.

MC3T3-E1 cells were procured from the Cell Bank of the Chinese Academy of Sciences (Shanghai, China). Phosphate-buffered saline (PBS), fetal bovine serum (FBS), alpha-minimum essential medium (α-MEM), penicillin, and streptomycin were obtained from HyClone. The cell proliferation reagent, 3-(4,5-Dimethyl-2-thiazolyl)-2,5-diphenyl-2-h-tetrazolium bromide (MTT), and estradiol were sourced from Sigma-Aldrich (St. Louis, MO, USA). Alkaline phosphatase (ALP) activity, tartrate-resistant acid phosphatase (TRAP) assay kits, cell cycle and apoptosis detection kits, and Alizarin Red S staining kits were acquired from Beyotime (Shanghai, China). ELISA kits for the detection of receptor activator of nuclear factor-κB ligand (RANKL), osteoprotegerin (OPG), and osteocalcin (OCN) were provided by MLBIO Biotechnology (Shanghai, China). Reagents for measuring inorganic phosphorus and calcium concentrations were purchased from Nanjing Jiancheng Bioengineering Institute.

2.2 Assessment of Osteogenic Activity in Ovariectomized C57BL/6J Mice

Based on the method of Yang et al. [20] with modifications. Female C57BL/6J mice (20-22 g, 8-10 weeks old) were obtained from Liaoning Changsheng Biotechnology Co., Ltd. The animal procedures were performed in strict accordance with the guidelines of the National Institutes of Health. Mice were maintained under standardized conditions (22-25℃, 50-60% humidity) with regulated 12 h light/dark cycles, in compliance with the Animal Ethics Committee standards of Dalian University of Technology. Standard chow was provided ad libitum.

The experimental cohort was divided into five groups (n=10 per group). Mice in the sham-operated group (Sham) underwent anesthesia followed by a surgical procedure to remove fat tissue near the ovaries. Mice in the remaining groups underwent ovariectomy (OVX) and were allowed a one-week recovery period post-surgery [16]. Following recovery, treatments were administered via gavage, except for the Sham and OVX control groups. The positive control group (OVX + E2) received bi-weekly estrogen injections (0.1 mg/kg), the high-dose group (OVX + CWPH) was gavaged with 300 mg/kg/day of colostrum whey protein, and the low-dose group (OVX + CWPL) received 30 mg/kg/day for three months.

At the end of the experimental period, the mice were euthanized, and blood samples were collected immediately. Serum levels of osteoprotegerin (OPG), receptor activator of nuclear factor-κB ligand (RANKL), alkaline phosphatase (ALP), tartrate-resistant acid phosphatase (TRAP), calcium (Ca), and inorganic phosphate (Pi) were measured [21]. Following dissection, right femurs were fixed in 4% paraformaldehyde and decalcified using 8% EDTA. The processed samples were paraffin-embedded, sectioned, and stained with H&E, TRAP, and Masson's trichrome to evaluate osteoclast activity and collagen distribution histologically [22].

2.3 Micro-Computed Tomography (Micro-CT) Imaging Analysis.

The left femur from each mouse was collected for microstructural analysis using a micro-CT system. The femur was then reconstructed from the dataset using Sky-scan NR econ software. The region of interest (ROI) was defined, and the trabecular bone within this region was modeled in three dimensions using CT vol software. Bone morphology parameters and microstructural indices, including bone density, bone volume, tissue volume, bone surface area/volume ratio, trabecular thickness, trabecular number, trabecular separation, and trabecular pattern factor, were quantified with Sky-scan CT analyzer software to assess bone microarchitecture in the mice [23].

2.4 Cell Culture and MTT Assay

MC3T3-E1 cells were cultured in α-MEM supplemented with 10% fetal bovine serum, 100 U/mL penicillin, and 100 μg/mL streptomycin, and maintained at 37°C in a 5% CO_2 incubator. Upon reaching 80% confluence, cells were passaged by aspirating the spent medium and dissociating with 1 mL of 0.25% trypsin-EDTA. After a brief incubation, the cells were washed twice with PBS. Digestion was terminated by adding complete medium, and the cells were gently resuspended. After transferring to a 15 mL conical tube, centrifugation at 1000 r/min for 5 min yielded a cell pellet. The pellet was resuspended in fresh medium and sub-cultured at a 1:2 ratio into new culture flasks.

For the MTT assay, MC3T3-E1 cells were seeded in 96-well plates (5×10^4 cells/well) and incubated for 24 h to allow adherence. The cells were then exposed to CWP at concentrations of 0, 50, and 200 μg/mL for 24, 48, and 72 h. After treatment, 10 μL of MTT solution (5 mg/mL) was added to each well and incubating for 4 h at 37°C. Following incubation, the medium was removed, and 150 μL of dimethyl sulfoxide (DMSO) was added to dissolve the formazan crystals. The cell suspension was gently vortexed to achieve full solubilization. Absorbance was measured at 570 nm using a microplate reader, and cell viability was calculated based on the absorbance values.

2.5 Osteoblast Differentiation and Mineralization Assays.

MC3T3-E1 cells were seeded at a density of 5×10^4 cells/well in a 12-well plate and cultured for 24 h. CWP at concentrations of 0, 50 and 200 μg/mL was then added to the differentiation medium, which consisted of α-MEM complete medium, 50 μg/mL ascorbic acid, and 10 mmol/L β-glycerophosphate. The group without CWP served as the blank control. The cells were induced for 14 days, with medium changes

every other day. At the end of the incubation period, the culture medium was harvested for extracellular ALP activity quantification using a commercial assay kit , following the manufacturer's protocol. After two washes with PBS, the cells were stained with the alkaline phosphatase staining kit and examined under a microscope [24].

For the mineralization assay, after 21 days, the medium was discarded, and the wells were washed with PBS. Each well was treated with 1 mL of 4% paraformaldehyde for 30 min. After removal of paraformaldehyde, 0.2% alizarin red solution was added, and the cells were incubated for 20 min. The wells were washed three times with PBS, and mineralized osteoblast nodules were visualized by microscopy [25].

2.6 Real-Time Quantitative PCR Analysis

Cells were treated with CWP at concentrations of 0, 50, and 200 μg/mL for 72 h, as described in the cell culture method. Total RNA was extracted from cell cultures using the Eastep™ Super Total RNA Extraction Kit. cDNA synthesis was carried out using the FastKing One-Step De-Genomic cDNA First Strand Synthesis Premix Reagent. Real-time qPCR was conducted with a qTOWER2.2 fluorescence quantitative PCR system, with β-actin used as the housekeeping gene [26].

2.7 Western Blot Analysis.

Cells were treated with CWP at concentrations of 0, 50, and 200 μg/mL for 72 h, using the cell culture method described above. Protein extraction was performed using a lysis buffer containing PMSF and RIPA, and the protein concentration was quantified using the BCA Protein Assay Kit. The protein samples were separated by SDS-PAGE and transferred to a polyvinylidene fluoride (PVDF) membrane. Blocking was performed with 5% BSA for 2 h. After blocking, the PVDF membrane was incubated with primary and secondary antibodies, followed by signal development using a chromogenic solution. Protein bands were visualized with a gel imaging system and quantified through ImageJ 1.51 software [27].

2.8 Statistical Analysis

All experiments were conducted in triplicate, and the data are expressed as the mean ± standard deviation. Statistical analysis was performed using one-way analysis of variance (ANOVA) followed by Duncan’s post hoc test, conducted with GraphPad Prism 9.0 software, to compare the experimental results with those of the control group. A p-value of less than 0.05 was considered statistically significant.

Results

3.1 CWP Ameliorates Trabecular Microarchitecture and Bone Mineral Density (BMD) in Ovariectomized (OVX) Mice

To evaluate the therapeutic efficacy of CWP in estrogen deficiency-induced osteoporosis, OVX mice were administered low-dose (CWPL, 30 mg/kg/day) or high-dose (CWPH, 300 mg/kg/day) CWP via oral gavage for 12 weeks. Three-dimensional micro-computed tomography (μCT) analysis demonstrated marked trabecular bone loss in OVX mice, evidenced by a 31% reduction in bone BMD relative to sham-operated controls (**Fig. 1. B**). Trabecular microarchitectural parameters were similarly impaired, with significant

reductions in trabecular number (Tb.N, −23%) and thickness (Tb.Th, −29%), alongside a 41% increase in trabecular separation (Tb.Sp) (**Fig. 1. C-J**). CWP treatment induced dose-dependent restoration of trabecular integrity, with CWPH exhibiting maximal therapeutic efficacy: BMD increased by 33%, Tb.N by 46%, and Tb.Th by 60%, while Tb.Sp decreased by 22% compared to OVX controls. CWPH achieved near-normalization of trabecular metrics, whereas CWPL elicited intermediate restorative effects (BMD: +14%, Tb.N: +42%).

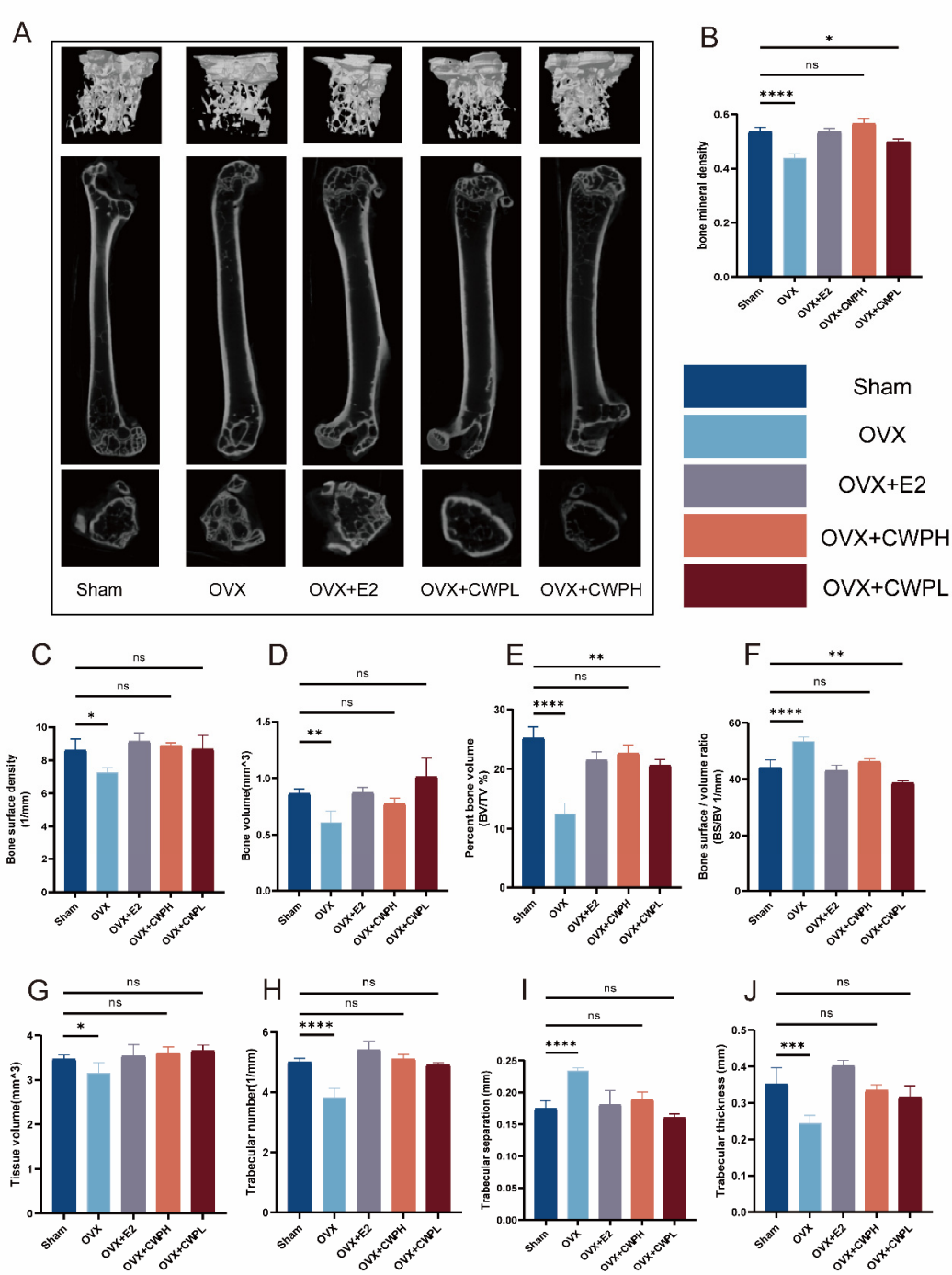

Fig. 1. CWP Improved osteogenesis in the femur of OVX mice. (A) Three-dimensional reconstruction of bone trabeculae with profiles (X-Z axis) and cross sections (X-Y axis). (B) Bone mineral density. (C) Bone surface density. (D) Bone volume. (E) Percent bone volume. (F) Bone surface/volume ratio. (G) Tissue volume. (H) Trabecular number (Tb.N). (I) Trabecular separation (Tb.Sp). (J) Trabecular thickness (Tb.Th). Sham: removal of mouse fat tissue group; OVX: removal of mouse ovaries group; OVX + CWPL: OVX mice with oral gavage of CWP at 30 mg/kg·day; OVX + CWPH: OVX mice with oral gavage of CWP at 300 mg/kg·day. Graphs represent the mean ± SD (n = 3). One-way ANOVA followed by Tukey's multiple comparisons test was performed; $^{ns}P > 0.05$, $^{*}P \leq 0.05$, $^{**}P \leq 0.01$, $^{****}P \leq 0.0001$.

Histomorphometric validation further substantiated μCT findings. Hematoxylin and eosin (H&E)-stained femoral sections revealed severe trabecular deterioration in OVX mice, characterized by fragmented, discontinuous trabeculae with diminished connectivity (**Fig. 2. H**). In contrast, CWP-treated cohorts maintained trabecular integrity, with CWPH mice displaying densely packed, interconnected trabecular networks comparable to sham controls. Masson's trichrome staining, which discriminates collagen fibers (blue) [22], confirmed significant collagen depletion in OVX bone (−65% vs. sham), while CWPH restored collagen content to 90% of sham levels (**Fig. 2. I**). Tartrate-resistant acid phosphatase (TRAP) staining identified a 3.2-fold elevation in osteoclast activity (TRAP-positive multinucleated cells) in OVX mice, which was attenuated by 66% in the CWPH group (**Fig. 2. J**), indicative of potent anti-resorptive activity.

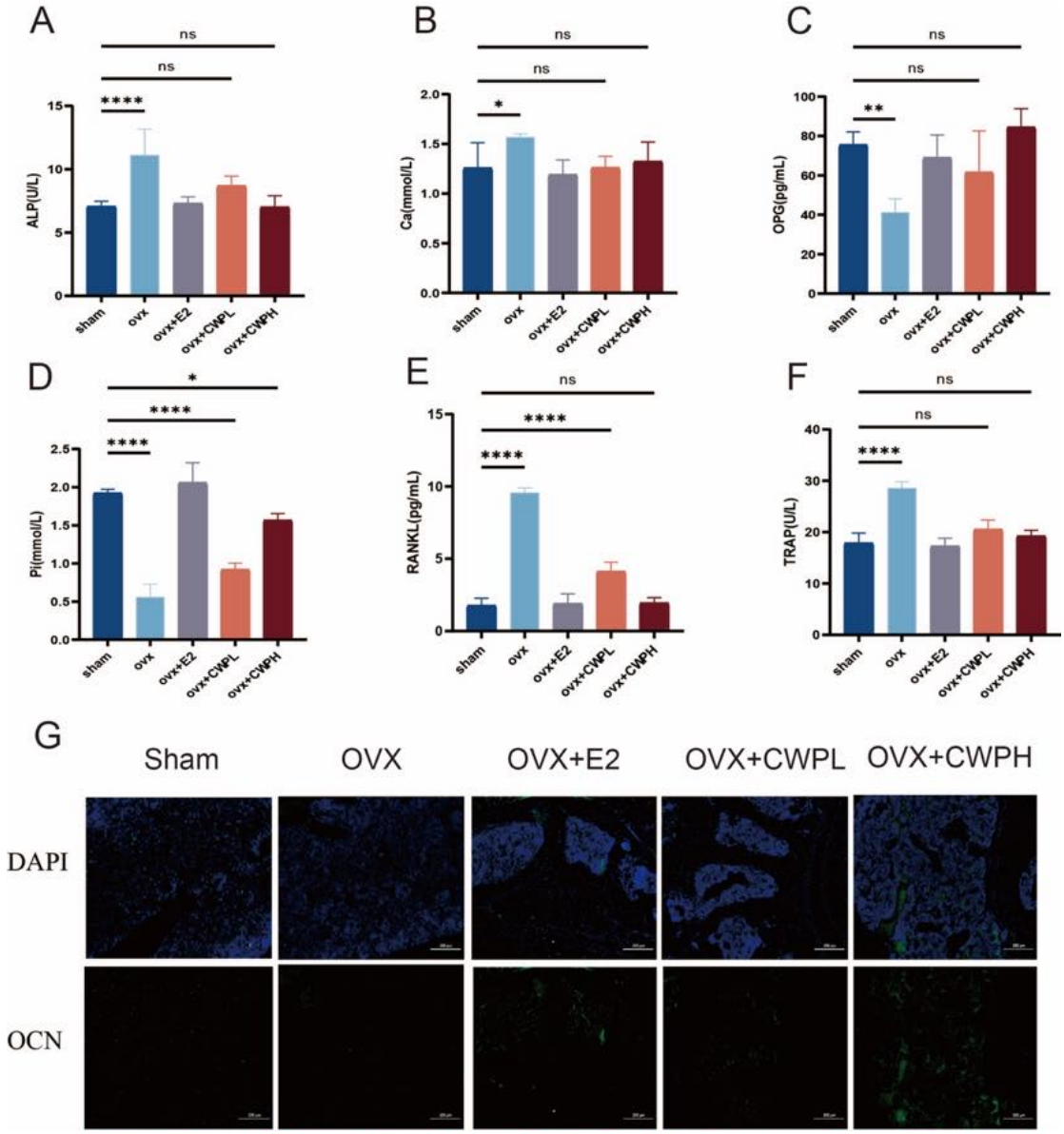

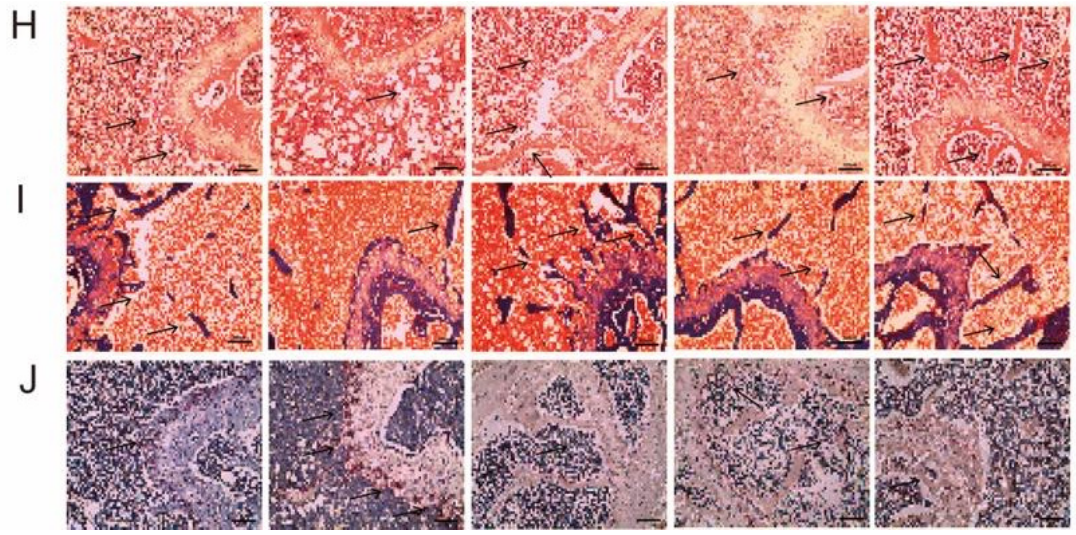

Fig. 2. Effect of CWP on serum biomarkers of bone formation in OVX mice. (A) ALP. (B) Ca. (C) OPG. (D) Pi. (E) RANKL. (F) TRAP. (G) OCN Expression map and fluorescence intensity analysis in bone tissue, Scale bar = 200 μm. (H) Hematoxylin and eosin (HE) staining of femur sections (scale bar: 200 μm) highlighting bone microstructure. (I) Masson staining of femoral sections (scale bar: 200 μm). (J) Tartrate-resistant acid phosphatase (TRAP) staining of osteoclasts (scale bar: 200 μm). Graphs represent the mean ± SD (n = 3). One-way ANOVA followed by Tukey's multiple comparisons test was performed; $^{ns}P > 0.05$, $^{*}P \leq 0.05$, $^{**}P \leq 0.01$, $^{****}P \leq 0.0001$.

3.2 CWP-Mediated Regulation of Bone Metabolic Markers to Restore Homeostasis

To evaluate the therapeutic effects of CWP on bone remodeling dynamics, serum biomarkers of bone turnover were quantitatively analyzed. ALP activity, a key marker of osteoblast function, was significantly elevated in OVX mice compared to sham-operated controls ($P < 0.05$; **Fig. 2. A**). CWP administration dose-dependently restored ALP activity, with high- and low-dose groups exhibiting reductions of 50% and 47%, respectively, indicative of enhanced osteoblast-mediated bone formation.

TRAP activity, a hallmark of osteoclast activity, was significantly elevated in OVX mice ($P < 0.01$; **Fig. 2. F**). CWP treatment suppressed TRAP activity by 31% (CWPH) and 28% (CWPL), consistent with attenuated osteoclast-driven bone resorption. Furthermore, the RANKL/OPG ratio, a pivotal regulator of osteoclast differentiation, was significantly elevated in OVX mice but normalized following CWP intervention. High-dose CWP reduced RANKL levels by 30% while increasing osteoprotegerin (OPG) concentrations by 91% (**Fig. 2. E**), collectively demonstrating inhibition of osteoclastogenesis. Serum calcium (Ca^{2+}) and inorganic phosphate (Pi) levels, which were dysregulated in OVX mice, were restored to physiological levels in CWP-treated groups (**Fig. 2. B-D**). These findings highlight CWP's ability to reestablish mineral homeostasis, a critical factor in preserving skeletal integrity.

3.3 CWP Modulated the Hepatic-Bone Axis

Emerging evidence underscores the hepatic-bone axis as a pivotal regulator of bone homeostasis. In OVX mice, hepatic expression of protein phosphatase 2A catalytic subunit alpha (PP2ACα) was significantly upregulated, promoting pathological cholesterol deposition in bone tissue and suppressing osteoblast-mediated mineralization ($P < 0.05$; **Fig. 3. C**). CWP treatment restored this dysregulation, reducing hepatic PP2ACα expression by 91% in the high-dose group (CWPH), thereby facilitating cholesterol efflux from bone to liver. Concurrently, CWP administration robustly upregulated lecithin-cholesterol

acyltransferase (LCAT) expression in the liver (9.3-fold increase in CWPH; **Fig. 3. D**), enhancing reverse cholesterol transport. In bone tissue, immunohistochemical analysis revealed that CWP intervention markedly elevated the expression of bone morphogenetic protein-2 (BMP-2) and runt-related transcription factor 2 (RUNX-2), key transcriptional regulators of osteoblast differentiation. Compared to OVX controls, the CWPH group exhibited a 1.4-fold increase in BMP-2 and a 1.8-fold increase in RUNX-2 expression (**Fig. 3. A-B**). These results demonstrate CWP's dual therapeutic mechanism: resolving systemic cholesterol trafficking disruptions and directly enhancing osteoblast activity to restore skeletal integrity.

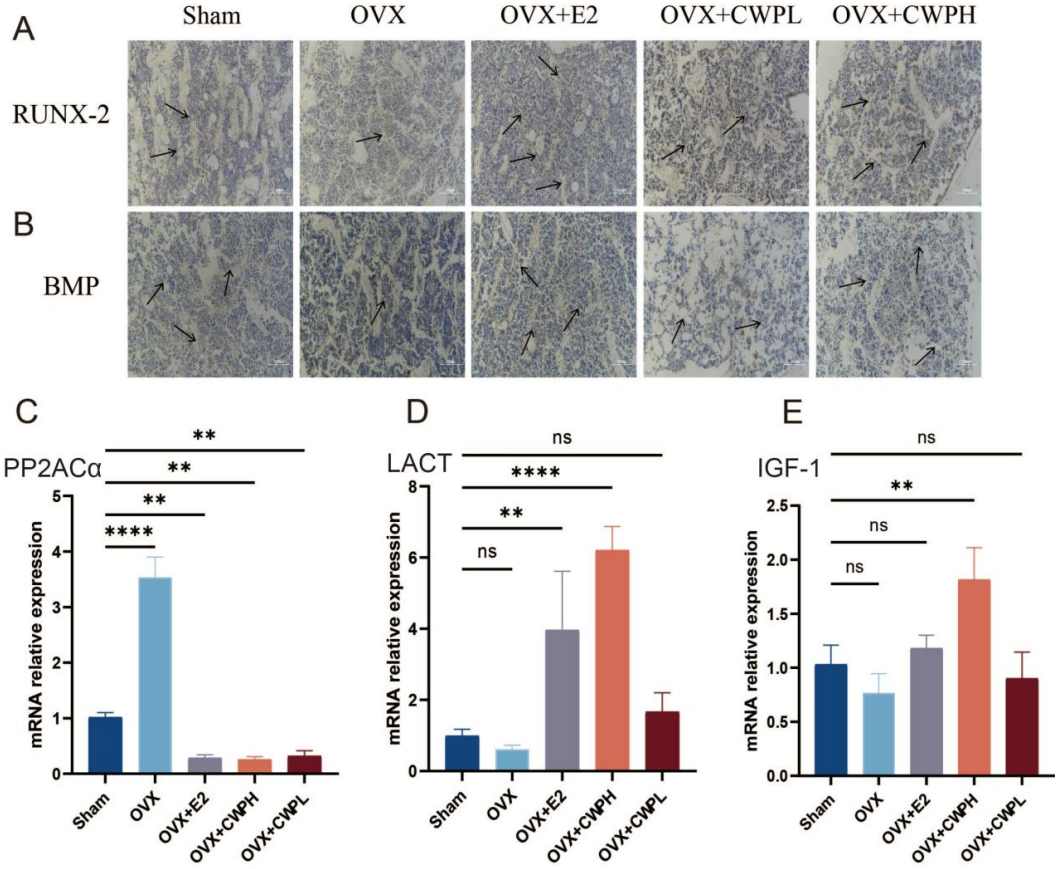

Fig. 3. CWP Regulated hepatic-bone axis mediators associated with osteogenic activity in OVX mice
(A) RUNX-2 representative images of IHC staining. (B) BMP representative images of IHC staining. (C) qRT-PCR analysis of PP2ACα mRNA expression in the liver of OVX mice. (D) qRT-PCR analysis of LACT mRNA expression in the liver of OVX mice. (E) qRT-PCR analysis of IGF-1 mRNA expression in the liver of OVX mice. Graphs represent the mean ± SD (n = 3). A one-way ANOVA followed by Tukey's multiple comparisons test was conducted; $^{ns}P > 0.05$, $^{*}P \leq 0.05$, $^{**}P \leq 0.01$, $^{****}P \leq 0.0001$.

3.4 CWP Enhances Osteogenic Activity via Proliferation, Differentiation, and Matrix Mineralization

In vitro experiments using MC3T3-E1 preosteoblasts were performed to evaluate CWP's direct osteogenic effects. Proliferation assays showed a concentration-dependent increase in cell viability, with a 23% enhancement at 200 μg/mL CWP after 72 h (**Fig. 4. A-C**). Quantitative PCR analysis confirmed significant upregulation of MAPK pathway components, ERK1/2 and JNK ($P < 0.05$; **Fig. 4. D-F**), demonstrating CWP-induced stimulation of mitogen-activated protein kinase signaling. CWP enhanced osteoblast differentiation, as indicated by a 1.3-fold increase in alkaline phosphatase (ALP) activity at 200 μg/mL (**Fig. 5. B**). Transcriptional analysis revealed pronounced upregulation of osteogenic markers: bone morphogenetic protein-2 (BMP-2) and runt-related transcription factor 2 (RUNX-2) expression increased by

3.4-fold and 5.4-fold, respectively (**Fig. 5. C-E**). Elevated β-catenin expression further suggested synergistic activation of WNT/β-catenin and BMP/Smad signaling pathways [28].

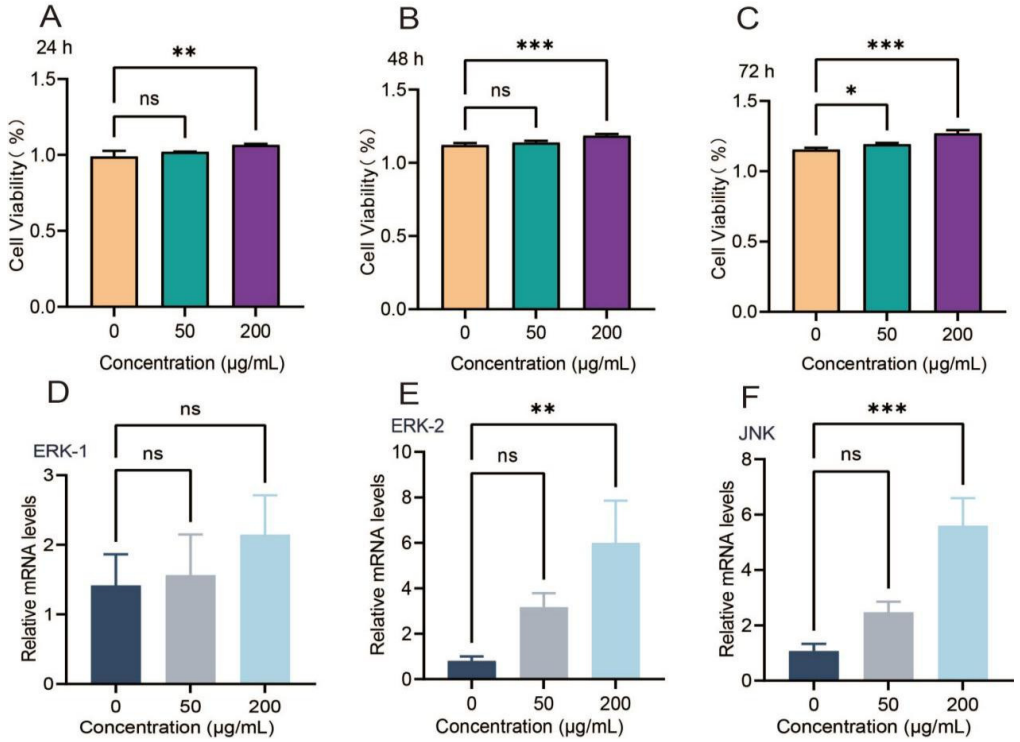

Fig. 4. Dose-dependent stimulation of MC3T3-E1 preosteoblast proliferation by CWP. (A-C) Effect of different concentrations of CWP on the proliferative activity of MC3T3-E1 at 24 h, 48 h, and 72 h. n = 3 per group. (D-F) qRT-PCR analysis of ERK1/2 and JNK mRNA expression in MC3T3-E1 after treatment with different concentrations of CWP. Graphs represent the mean ± SD (n = 3). One-way ANOVA followed by Tukey's multiple comparisons test was performed; $^{ns}P > 0.05$, $^{*}P \leq 0.05$, $^{**}P \leq 0.01$, $^{****}P \leq 0.0001$.

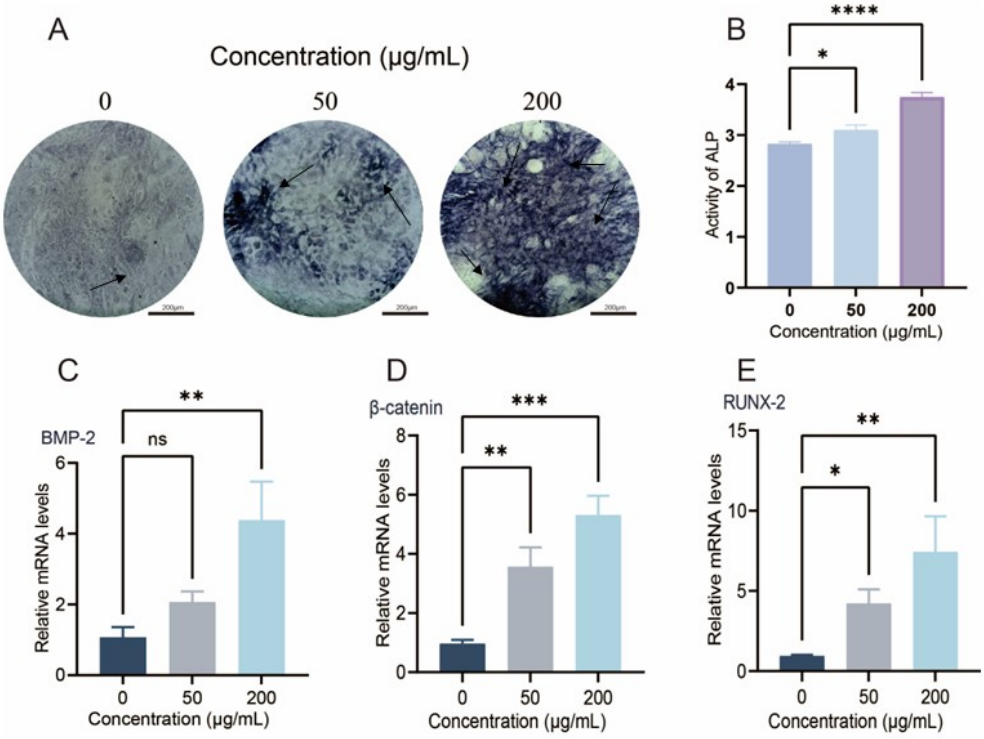

Fig. 5. CWP enhanced MC3T3-E1 preosteoblast differentiation in a concentration-dependent manner (A) Representative images of cell differentiation (Scale bar: 200 μm). (B) ALP Mars quantitative analysis. (C-E) qRT-PCR analysis of BMP-2, β-catenin, and RUNX-2 mRNA expression in differentiated osteoblasts treated with different concentrations of CWP. Graphs represent the mean ± SD (n = 3). One-way ANOVA followed by Tukey's multiple comparisons test was performed; $^{ns}P > 0.05$, $^{*}P \leq 0.05$, $^{**}P \leq 0.01$, $^{****}P \leq 0.0001$.

Mineralization assays validated CWP's ability to promote late-stage osteogenic maturation. Alizarin Red S staining demonstrated a 2.1-fold increase in mineralized nodule formation at 200 μg/mL CWP (**Fig. 6. A-B**). Expressions of bone matrix proteins - bone sialoprotein (BSP), collagen type I (COL-I), and osteocalcin (OCN) were significantly upregulated, with BSP levels rising by 4.5-fold and COL-I/OCN by 4-fold ($P < 0.01$; **Fig. 6. C-E**). Together, these findings illustrate CWP's comprehensive osteogenic effects, spanning early proliferation, differentiation, and terminal matrix mineralization.

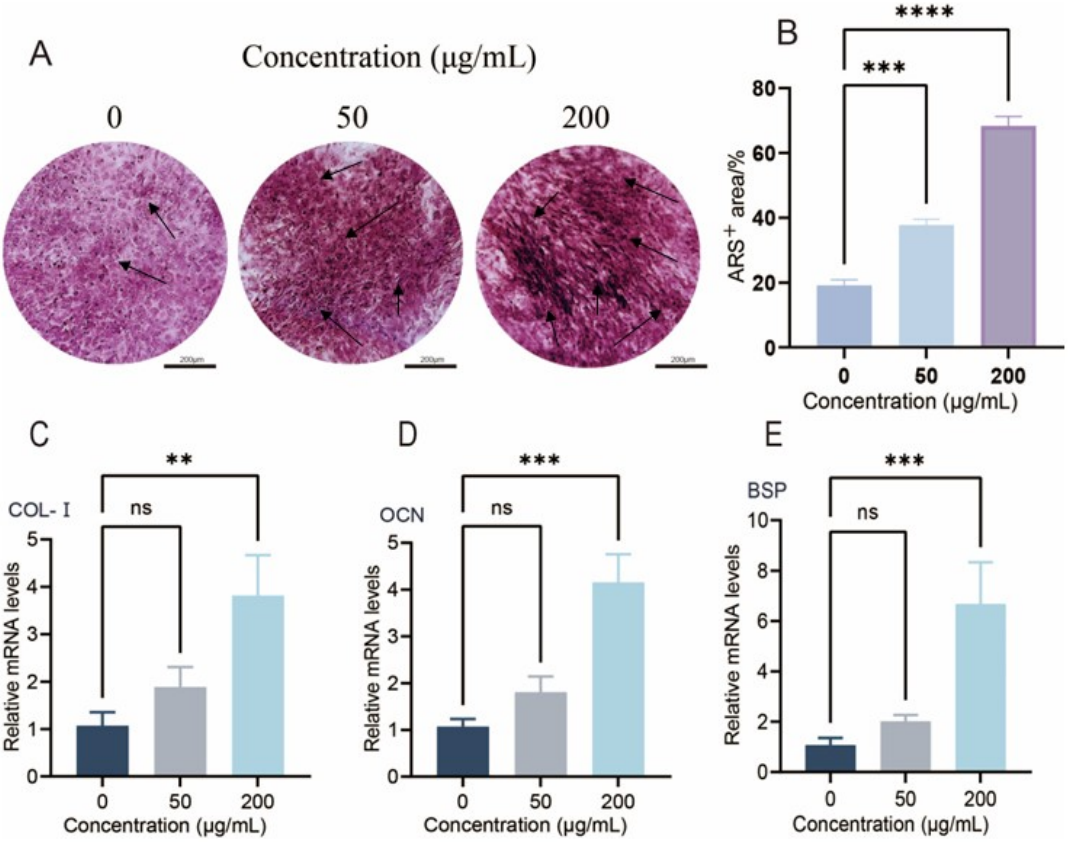

Fig. 6. CWP promoted osteogenic mineralization in MC3T3-E1 cells. (A) Representative images of cell mineralization (Scale bar: 200 μm). (B) Quantitative analysis of ARS^+ regions. (C-E) qRT-PCR analysis of COL-I, OCN, and BSP mRNA expression in mineralized osteoblasts treated with different concentrations of CWP. Graphs represent the mean ± SD (n = 3). One-way ANOVA followed by Tukey's multiple comparisons test was performed; $^{ns}P > 0.05$, $^{*}P \leq 0.05$, $^{**}P \leq 0.01$, $^{****}P \leq 0.0001$.

3.5 CWP Activated BMP/Smad, WNT/β-Catenin, and MAPK Pathways to Promote Osteogenesis

Bone morphogenesis is regulated by tightly coordinated signaling pathways that govern osteoblast proliferation, differentiation, and extracellular matrix synthesis [29]. Western blot analysis revealed that CWP robustly activated key osteogenic pathways, BMP/Smad, WNT/β-catenin, and MAPK, central to skeletal development. BMP-2, a master regulator of osteoblast differentiation and matrix production, exhibited dose-dependent upregulation, with a 2-fold increase in expression at 200 μg/mL CWP compared to untreated controls (**Fig. 7. A**). BMP-2 ligand-receptor binding triggers canonical Smad1/5/8 phosphorylation, enabling nuclear translocation of phosphorylated Smad complexes. These complexes synergize with RUNX-2 to transactivate osteogenic markers, including alkaline phosphatase (ALP), collagen type I (COL-I), and osteocalcin (OCN), consistent with their elevated expression in CWP-treated cells (**Fig. 6. C-E**).

CWP also upregulated SP7 (Osterix), a transcription factor critical for osteoblast lineage progression, with a 1.5-fold increase at the highest dose (**Fig. 7. E**). SP7, functioning downstream of RUNX-2, drives terminal osteoblast maturation and bone matrix protein synthesis. The coordinated induction of SP7 and RUNX-2 underscores CWP's ability to activate hierarchical transcriptional networks essential for osteogenesis.

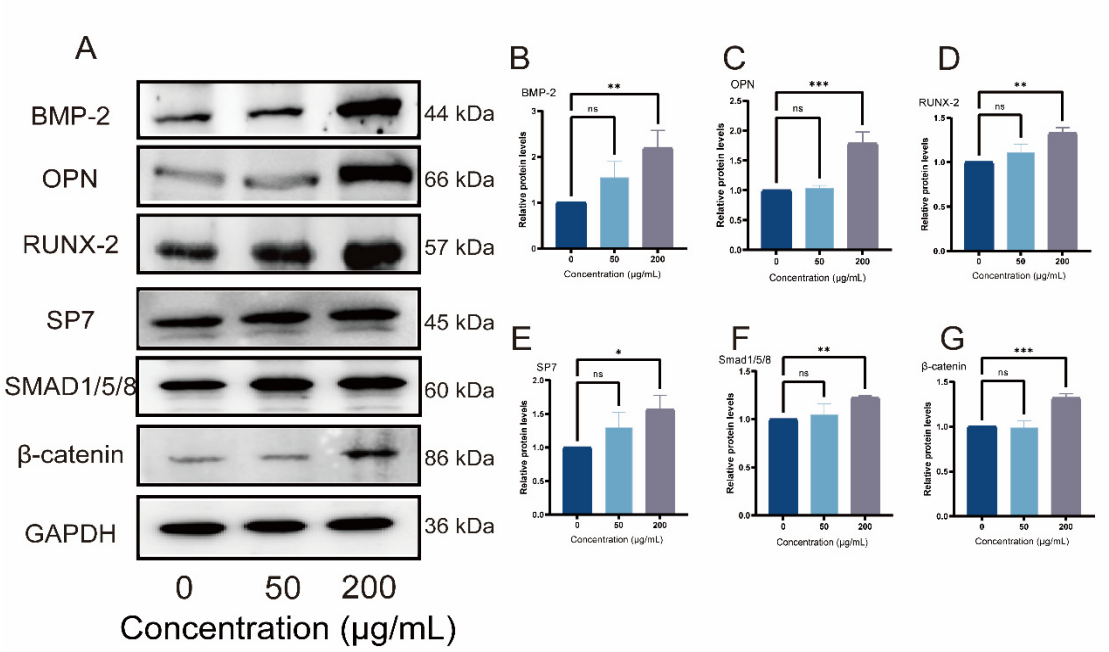

Fig. 7. CWP upregulated osteogenic regulatory protein expression (e.g., BMP-2, RUNX-2, β-catenin) in a concentration-dependent manner. (A) Western blot analysis of BMP-2, OCN, RUNX-2, SP7, Smad1/5/8, and β-catenin protein levels in osteoblasts treated with different concentrations of CWP. (B-G) Relative expression of BMP-2, OCN, RUNX-2, SP7, Smad1/5/8, and β-catenin as a percentage of GAPDH. Graphs represent the mean ± SD (n = 3). One-way ANOVA followed by Tukey's multiple comparisons test was performed; $^{ns}P > 0.05$, $^{*}P \leq 0.05$, $^{**}P \leq 0.01$, $^{****}P \leq 0.0001$.

Furthermore, CWP enhanced WNT/β-catenin signaling, a pivotal regulator of osteoblast activity. β-catenin expression increased 1.3-fold at 200 μg/mL CWP (**Fig. 7. G**). WNT-mediated stabilization of β-catenin facilitates its cytoplasmic accumulation and nuclear translocation, where it binds TCF/LEF transcription factors to upregulate osteogenic targets such as RUNX-2. The concurrent upregulation of β-catenin and RUNX-2 suggests synergistic crosstalk between WNT and BMP pathways, amplifying CWP-induced osteogenesis.

MAPK signaling, involving ERK1/2 and JNK cascades, contributed to CWP's osteogenic effects. As shown earlier in **Fig. 4. D-F**, CWP elevated ERK1/2 and JNK transcript levels, indicating pathway activation. ERK1/2 signaling promotes osteoblast proliferation via cyclin D1 induction and enhances differentiation through RUNX-2 phosphorylation, boosting its transcriptional activity. This dual role aligns with the observed upregulation of RUNX-2 and differentiation markers in CWP-treated cells.

Beyond isolated pathway activation, CWP coordinates inter-pathway crosstalk to enhance osteogenesis. BMP and WNT pathways converge through β-catenin stabilization, while MAPK signaling potentiates Smad transcriptional activity, amplifying BMP outputs [30]. This synergism underlies the robust osteogenic response to CWP. By simultaneously engaging BMP/Smad, WNT/β-catenin, and MAPK axes, CWP employs a

polypharmacological mechanism distinct from single-pathway agents. Such multi-targeted activation synchronizes osteoblast proliferation, matrix synthesis, and mineralization, ensuring spatiotemporal coordination of bone formation.

4. Discussion

This study investigated the therapeutic potential of CWP in mitigating estrogen deficiency-induced osteoporosis, with a particular focus on bone remodeling and systemic metabolic regulation. Using both in vivo and in vitro models, the findings demonstrate that CWP improved bone microstructure, modulated metabolic biomarkers, and activated key molecular pathways, highlighting its multifaceted role in bone homeostasis.

In the OVX mouse model, which replicates postmenopausal osteoporosis, the results revealed significant reductions in BMD, trabecular thickness (Tb.Th), and trabecular number (Tb.N), along with increasing trabecular separation (Tb.Sp). BMD is a critical indicator of skeletal strength and fracture risk, while Tb.N reflects trabecular density and structural integrity. In osteoporotic patients, the number of trabeculae decreases, leading to increased bone fragility and higher fracture risk [31,32]. The high-dose CWP (CWPH) treatment significantly reversed these deficits, with BMD increasing by 33%, Tb.N increasing by 46%, and Tb.Th increasing by 60%, while Tb.Sp decreasing by 22% compared to untreated OVX mice (**Fig. 1 B-J**). These findings are consistent with studies that show the potential of natural peptides, like CWP, to restore bone mass and improve microarchitecture in osteoporotic models [33]. Histological analysis confirmed these structural improvements, revealing compact trabeculae, reduced osteoclast activity (66% suppression in TRAP+ cells; **Fig. 2. J**), and restored collagen content (90% of sham levels; **Fig. 2. I**). These results underscore CWP's dual ability to enhance bone formation and suppress resorption, which aligns with recent studies highlighting the importance of balancing both osteoblast and osteoclast activities in osteoporosis treatment [34].

CWP induced a 1.5-fold increase in ALP activity, a marker of osteoblast activity and bone mineralization, indicating enhanced osteoblast-mediated mineralization, consistent with previous findings on the role of ALP in osteogenesis [35-37] (**Fig. 2. A**). RANKL/OPG ratio, a driver of osteoclastogenesis, was normalized, leading to a 31% reduction in TRAP activity (**Fig. 2. F**). Serum calcium and phosphate levels, which are critical for bone mineralization, were restored to physiological ranges (**Fig. 2. B-D**). These findings align with studies on other bioactive peptides, such as mussel-derived peptides, which also modulated the RANKL/OPG axis and improved bone turnover[38,39]. However, CWP's unique ability to integrate osteoblast activation and osteoclast suppression simultaneously distinguishes it from conventional antiresorptive therapies, which typically focus on either enhancing bone formation or inhibiting resorption [40,41].

Beyond its local effects on bone metabolism, CWP demonstrated systemic metabolic effects via modulation of the hepatic-bone axis. Estrogen deficiency is known to disrupt this axis, leading to cholesterol accumulation in bone tissue, which impairs osteoblast function by downregulating BMP-2 and RUNX-2 expression [42,43]. In this study, CWP treatment significantly modulated key hepatic factors. PP2ACα

expression was reduced by 91%, and LCAT expression increased by 9.3-fold (**Fig. 3. C-D**), facilitating cholesterol transport from bone to liver. Concurrently, bone tissue exhibited a 1.4-fold and 1.8-fold increase in BMP-2 and RUNX-2 expressions, respectively (**Fig. 3. A-B**), transcription factors essential for osteogenesis. This dual regulation suggests that CWP restored bone health not only by directly targeting osteoblasts but also by addressing systemic metabolic imbalances, as supported by studies showing that metabolic dysregulation could impair bone health [44].

In MC3T3-E1 preosteoblasts, CWP enhanced cell proliferation in a dose-dependent manner, with a 23% increase in viability at 200 μg/mL (**Fig. 4. A-C**). This effect was linked to the activation of the MAPK pathway, as evidenced by increased phosphorylation of ERK1/2 and JNK (**Fig. 4. D-F**) [45,46]. CWP also amplified osteoblast differentiation, with a 2.3-fold increase in ALP activity and significant upregulation of BMP-2, RUNX-2 and β-catenin (**Fig. 5. C-E).** These molecular changes resulted in a 3-fold increase in mineralized nodules (**Fig. 6. A-B)** and elevated expression of bone matrix proteins, including bone sialoprotein (BSP), collagen type I (COL-I), and osteocalcin (OCN) (**Fig. 6. C-E**). This aligns with previous studies indicating that WNT/β-catenin and BMP/Smad signaling are key mediators of osteogenesis [47]. The upregulation of these proteins underscored CWP's effectiveness in promoting all stages of osteoblast activity, from proliferation to late-stage mineralization.

The activation of BMP/Smad and WNT/β-catenin signaling pathways by CWP is very important in promoting osteogenesis, as it enhanced bone formation and repair. This dual activation led to increased BMP-2 expression, which in turn drived Smad1/5/8 phosphorylation (**Fig. 7. A**), and stabilized β-catenin, enhancing WNT-mediated transcription (**Fig. 7. B-G**). The synergistic activation of these pathways, along with MAPK, underscored CWP's potential in promoting osteogenesis from progenitor proliferation to terminal mineralization. This mechanism aligns with existing literatures those highlight the importance of these pathways in bone formation and repair [48-50].

Collectively, this study positions CWP as a comprehensive therapeutic agent for osteoporosis, offering multiple advantages over conventional antiresorptive treatments. Its ability to promote osteoblast activity, inhibit osteoclast resorption, and correct metabolic dysfunctions through hepatic-bone axis modulation makes it a promising candidate for addressing the multifactorial pathophysiology of osteoporosis. By integrating direct osteoblast activation with osteoclast suppression and systemic metabolic correction, CWP provides a more holistic approach to managing postmenopausal bone loss, which often focus on either bone formation or resorption alone. These results contribute to the growing evidence supporting the use of bioactive peptides in bone health and open the door for future clinical applications of CWP in osteoporosis management.

5. Conclusion

This study demonstrates that CWP mitigated osteoporosis through osteogenic stimulation, anti-resorptive activity, and modulation of the hepatic-bone axis. In OVX mice, CWP restored trabecular bone microarchitecture by promoting osteoblast differentiation via coordinated modulation of BMP/Smad, WNT/β-catenin, and MAPK signaling pathways and suppressing osteoclastogenesis through normalization of

the RANKL/OPG ratio. At the systemic level, CWP ameliorated estrogen deficiency-induced metabolic dysregulation by downregulating PP2ACα and upregulating LCAT expression, facilitating cholesterol efflux from bone tissue and reinstating BMP-2- and RUNX-2-dependent mineralization. Unlike conventional antiresorptive therapies, CWP coordinated bone formation and resorption while rectifying systemic metabolic imbalances, thereby providing a multifactorial therapeutic strategy for postmenopausal osteoporosis. Translation to clinical applications necessitates comprehensive preclinical validation of its long-term efficacy and safety in physiologically relevant models.

Declaration of competing interest

The authors declare that they have no conflicts of interest regarding the research presented in this manuscript.

Data availability

The data will be made available upon request.

Acknowledgment

This research was funded by the National Key Research and Development Program of China (2024YFF1106000), Guangdong Science and Technology Plan Projects (2023A0505050117), and the Guangdong Basic and Applied Basic Research Foundation (2023B1515040014).

References

[1] S.S. Amarnath, V. Kumar, S.L. Das, Classification of Osteoporosis, JOIO. 57 (2023) 49–54. https://doi.org/10.1007/s43465-023-01058-3.

[2] C. Geyer, Postmenopausal Osteoporosis: The Role of Lifestyle in Maintaining Bone Mass and Reducing Fracture Risk, Am J Lifestyle Med. 11 (2017) 125–128. https://doi.org/10.1177/1559827616682938.

[3] D.M. Black, C.J. Rosen, Clinical Practice. Postmenopausal Osteoporosis, N Engl J Med. 374 (2016) 254–262. https://doi.org/10.1056/NEJMcp1513724.

[4] K.E. Ensrud, C.J. Crandall, Osteoporosis, Ann. Intern. Med. 168 (2018) 306–307. https://doi.org/10.7326/L17-0587.

[5] S.W. Cheatham, W.J. Hanney, M.J. Kolber, et al., Osteoporosis: Exercise Programming Insight for the Sports Medicine Professional, Strength & Conditioning Journal. 39 (2017) 2. https://doi.org/10.1519/SSC.0000000000000302.

[6] P.A. Anderson, B.A. Freedman, W.T. Brox, et al., Osteoporosis: Recent Recommendations and Positions of the American Society for Bone and Mineral Research and the International Society for Clinical Densitometry, J. Bone Jt. Surg., Am. Vol. 103 (2021) 741–747. https://doi.org/10.2106/JBJS.20.01248.

[7] X.W. Yao, H.D. Liu, M.X. Ren, et al., Aloe polysaccharide promotes osteogenesis potential of adipose-derived stromal cells via BMP-2/Smads and prevents ovariectomized-induced osteoporosis, Mol. Biol. Rep. 49 (2022) 11913–11924. https://doi.org/10.1007/s11033-022-08003-x.

[8] Y. Jin, B.H. Zhou, J. Zhao, et al., Fluoride-induced osteoporosis via interfering with the RANKL/RANK/OPG pathway in ovariectomized rats: Oophorectomy shifted skeletal fluorosis from osteosclerosis to osteoporosis, Environ. Pollut. 336 (2023) 122407. https://doi.org/10.1016/j.envpol.2023.122407.

[9] Z. Chen, D. Liu, X. Tang, et al., Sea cucumber enzymatic hydrolysates relieve osteoporosis through OPG/RANK/RANKL system in ovariectomized rats, Food Biosci. 46 (2022) 101572. https://doi.org/10.1016/j.fbio.2022.101572.

[10] X.F. He, L. Zhang, C.H. Zhang, et al., Berberine alleviates oxidative stress in rats with osteoporosis through receptor activator of NF-kB/receptor activator of NF-kB ligand/osteoprotegerin (RANK/RANKL/OPG) pathway, Bosnian J. Basic Med. Sci. 17 (2017) 295–301. https://doi.org/10.17305/bjbms.2017.2596.

[11] X. Wang, Z. Qu, S. Zhao, et al., Wnt/β-catenin signaling pathway: proteins' roles in osteoporosis and cancer diseases and the regulatory effects of natural compounds on osteoporosis, Molecular Medicine. 30 (2024) 193. https://doi.org/10.1186/s10020-024-00957-x.

[12] A.K. Nussler, B. Wildemann, T. Freude, et al., Chronic CCl4 intoxication causes liver and bone damage similar to the human pathology of hepatic osteodystrophy: a mouse model to analyse the liver-bone axis, Arch. Toxicol. 88 (2014) 997–1006. https://doi.org/10.1007/s00204-013-1191-5.

[13] Y. Kaçar, H. Batmaz, Evaluation of the differences in proteomics of high-quality bovine colostrum and low-quality bovine colostrum, Vet. Med. Sci. 9 (2023) 2852–2861. https://doi.org/10.1002/vms3.1274.

[14] B. Liu, L. Sun, Y. Zhuang, Protective effects of tilapia (Oreochromis niloticus) skin gelatin hydrolysates on osteoporosis rats induced by retinoic acid, Food Sci. Hum. Wellness. 11 (2022) 1500–1507. https://doi.org/10.1016/j.fshw.2022.06.007.

[15] L. Zhang, S. Zhang, H. Song, et al., Effect of Collagen Hydrolysates from Silver Carp Skin (Hypophthalmichthys molitrix) on Osteoporosis in Chronologically Aged Mice: Increasing Bone Remodeling, Nutrients. 10 (2018) 1434. https://doi.org/10.3390/nu10101434.

[16] Y. Zhang, Y. Niu, C. Fu, et al., Preparation, identification and screening of anti-osteoporosis milk-derived peptides: Intervention effects in osteoporosis rats, Food Biosci. 62 (2024) 105120. https://doi.org/10.1016/j.fbio.2024.105120.

[17] A. Pant, J. Singh, R.P. Barnwal, et al., Theranostic Approach for the Management of Osteoporosis, Crit. Rev. Ther. Drug. Carrier. Syst. 40 (2023) 95–121. https://doi.org/10.1615/CritRevTherDrugCarrierSyst.2022043413.

[18] K.M. Beekman, A.G. Veldhuis-Vlug, M. den Heijer, et al., The effect of raloxifene on bone marrow adipose tissue and bone turnover in postmenopausal women with osteoporosis, BONEDL. 118 (2019) 62–68. https://doi.org/10.1016/j.bone.2017.10.011.

[19] K. Huang, S. Cai, T. Fu, et al., Wnt10b regulates osteogenesis of adipose-derived stem cells through Wnt/β-catenin signalling pathway in osteoporosis, Cell Proliferation. 57 (2024) e13522. https://doi.org/10.1111/cpr.13522.

[20] M. Yang, Z. Xu, D. Wu, et al., Characterizations and the Mechanism Underlying Osteogenic Activity of Peptides from Enzymatic Hydrolysates of *Stichopus japonicus*, J. Agric. Food Chem. 69 (2021) 15611-15623. https://doi.org/10.1021/acs.jafc.1c06028.

[21] S. Reddi, S.B. Mada, N. Kumar, et al., Antiosteopenic Effect of Buffalo Milk Casein-Derived Peptide (NAVPITPTL) in Ovariectomized Rats, Int. J. Pept. Res. Ther. 25 (2019) 1147–1158. https://doi.org/10.1007/s10989-018-9763-0.

[22] W.Liu, Y.Li, Y.An, et al., Yunnan Baiyao Might Mitigate Periodontitis Bone Destruction by Inhibiting Autophagy and Promoting Osteoblast Differentiation in vivo, ex vivo and in vitro, J. Inflamm. Res. (2024) 17:2271-2284. https://doi.org/10.2147/JIR.S454694.

[23] X. Zhou, S. Sun, Y. Chen, et al., Pulsed frequency modulated ultrasound promotes therapeutic effects of osteoporosis induced by ovarian failure in mice, Ultrasonics. 132 (2023) 106973. https://doi.org/10.1016/j.ultras.2023.106973.

[24] P. Kim, Y.J. Nam, W.J. Kim, et al.,Edgeworthia papyrifera Regulates Osteoblast and Osteoclast Differentiation In Vitro and Exhibits Anti-osteoporosis Activity in Animal Models of Osteoporosis, Planta Med. 85 (2019) 766–773. https://doi.org/10.1055/a-0942-1960.

[25] B. Kim, S.H. Lee, S.J. Song, et al., Protective Effects of Melon Extracts on Bone Strength, Mineralization, and Metabolism in Rats with Ovariectomy-Induced Osteoporosis, Antioxidants (Basel). 8 (2019) 306. https://doi.org/10.3390/antiox8080306.

[26] M. Yang, S. Su, S. Cheng, et al., Absorption and transport properties of a codfish-derived peptide and its protective effect on bone loss in ovariectomized mice, Food Funct. 15 (2024) 3496–3506. https://doi.org/10.1039/D3FO04819E.

[27] P. Shi, F. Fan, H. Chen, et al., A bovine lactoferrin-derived peptide induced osteogenesis via regulation of osteoblast proliferation and differentiation, J Dairy Sci. 103 (2020) 3950–3960. https://doi.org/10.3168/jds.2019-17425.

[28] J. Xi, Q. Li, X. Luo, et al., Epigallocatechin-3-gallate protects against secondary osteoporosis in a mouse model via the Wnt/β-catenin signaling pathway, Mol. Med. Rep. 18 (2018) 4555–4562. https://doi.org/10.3892/mmr.2018.9437.

[29] B. Raphael-Mizrahi, Y. Gabet, The Cannabinoids Effect on Bone Formation and Bone Healing, Curr Osteoporos Rep. 18 (2020) 433–438. https://doi.org/10.1007/s11914-020-00607-1.

[30] I.V. Zhivodernikov, T.V. Kirichenko, Y.V. Markina, et al., Molecular and Cellular Mechanisms of Osteoporosis, Int. J. Mol. Sci. 24 (2023) 15772. https://doi.org/10.3390/ijms242115772.

[31] F. Ozan, M. Pekedis, Ş. Koyuncu, et al., Micro-computed tomography and mechanical evaluation of trabecular bone structure in osteopenic and osteoporotic fractures, J Orthop Surg (Hong Kong). 25 (2017) 2309499017692718. https://doi.org/10.1177/2309499017692718.

[32] Y. Liu, Y. He, B. He, et al., The Anti-osteoporosis Effects of Natto on Bone Mineral Density in Perimenopausal Women, Curr. Med. Chem. 28 (2021) 5191–5200. https://doi.org/10.2174/0929867327666200306123140.

[33] C. Zhang, B. Du, G. Deng, et al., Anti-osteoporosis properties of phosphorylated collagen peptide-magnesium chelates in osteoblast MC3T3-E1 cells and ovariectomized mice. Chin. Med. J. 137(14) (2023) 1762-1764. https://doi.org/10.1097/cm9.0000000000002877.

[34] A. K. Kuril, K. M. Manchuri, S. Anand., Emerging Protein and Peptide Therapeutics for Osteoporosis: Advances in Anabolic and Catabolic Treatments. J. Pharm. Res. Int. 36(11) (2024) 85–102. https://doi.org/10.9734/jpri/2024/v36i117603.

[35] E. Bonucci, A. Nanci., Alkaline phosphatase and tartrate-resistant acid phosphatase in osteoblasts of normal and pathologic bone. Ital. J. Anat. Embryol. 106 (2001) 129–133.

[36] F. Sarac, F. Saygili. Causes of High Bone Alkaline Phosphatase. Biotechnol. Biotechnol. Equip. 21(2) (2007) 194–197. https://doi.org/10.1080/13102818.2007.10817444.

[37] S. Tournis, K. Makris. Clinical Use of Bone Turnover Markers in Osteoporosis. (2014). https://doi.org/10.1016/B978-0-12-801238-3.99538-2.

[38] G. Xia, Y. Zhao, Z. Yu, et al., Phosphorylated Peptides from Antarctic Krill (Euphausia superba) Prevent Estrogen Deficiency Induced Osteoporosis by Inhibiting Bone Resorption in Ovariectomized Rats. J. Agric. Food Chem. 63(43) (2015) 9550–9557. https://doi.org/10.1021/ACS.JAFC.5B04263.

[39] Z. Xu, F. Fan, H. Chen, et al., Absorption and transport of a Mytilus edulis-derived peptide with the function of preventing osteoporosis, Food Funct. 12 (2021) 2102–2111. https://doi.org/10.1039/D0FO02353A.

[40] N. A. Sims, K. W. Ng. Implications of Osteoblast-Osteoclast Interactions in the Management of Osteoporosis by Antiresorptive Agents Denosumab and Odanacatib. Current Osteoporosis Reports. 12(1) (2014) 98–106. https://doi.org/10.1007/S11914-014-0196-1

[41] A. Corrado, E. Sanpaolo, S. Di Bello, et al., Osteoblast as a target of anti-osteoporotic treatment. Postgrad. Med. 129(8) (2017) 858–865. https://doi.org/10.1080/00325481.2017.1362312

[42] S. Khosla, R. Pacifici. Estrogen Deficiency, Postmenopausal Osteoporosis, and Age-Related Bone Loss, Academic Press，Osteoporosis (Fourth Edition). (2013) 1113-1136 https://doi.org/10.1016/B978-0-12-415853-5.00046-7.

[43] L. Zhu, J. Shi, T.N. Luu, et al., Hepatocyte estrogen receptor alpha mediates estrogen action to promote reverse cholesterol transport during Western-type diet feeding, Mol. Metab. 8 (2018) 106–116. https://doi.org/10.1016/j.molmet.2017.12.012.

[44] M. D. Adhami, H. Rashid, H. Chen, et al., Loss of Runx2 in Committed Osteoblasts Impairs Postnatal Skeletogenesis. J. Bone Miner. Res. 30(1) (2015) 71–82. https://doi.org/10.1002/JBMR.2321.

[45] X.H. Hu, X.Y. Yang, J. Lian, et al., Moringa oleifera leaf attenuate osteoporosis in ovariectomized rats by modulating gut microbiota composition and MAPK signaling pathway, Biomed Pharmacother 161 (2023) 114434. https://doi.org/10.1016/j.biopha.2023.114434.

[46] W. Qin, Q. Shang, G. Shen, et al., Restoring bone-fat equilibrium: Baicalin's impact on P38 MAPK pathway for treating diabetic osteoporosis, Biomed. Pharmacother. 175 (2024) 116571. https://doi.org/10.1016/j.biopha.2024.116571.

[47] P. Arya, I. Saranya, N. Selvamurugan. Crosstalk between Wnt and bone morphogenetic protein signaling during osteogenic differentiation. World Journal of Stem Cells. 16(2) (2024) 102–113. https://doi.org/10.4252/wjsc.v16.i2.102.

[48] S. J. Bae, H. J. J. Kim, H. Y. Won,et al., Acceleration of osteoblast differentiation by a novel osteogenic compound, DMP-PYT, through activation of both the BMP and Wnt pathways. Scientific Reports. 7(1) (2017) 8455. https://doi.org/10.1038/S41598-017-08190-9

[49] G. Mbalaviele, S. Sheikh, J. P.Stains, et al., β-Catenin and BMP-2 Synergize to Promote Osteoblast Differentiation and New Bone Formation. J. Cell. Biochem. 94(2) (2005) 403–418. https://doi.org/10.1002/JCB.20253

[50] C. Chen, L. Huang, Y. Chen, et al., Hydrolyzed egg yolk peptide prevented osteoporosis by regulating Wnt/β-catenin signaling pathway in ovariectomized rats, Sci Rep. 14 (2024) 10227. https://doi.org/10.1038/s41598-024-60514-8.